Cation Control of Molecular Sieving by Flexible Li-containing Zeolite Rho

Magdalena M. Lozinska,[1] Enzo Mangano,[2] Alex G. Greenaway,[1] Robin Fletcher,[3] Stephen P. Thompson,[4] Claire A. Murray,[4] Stefano Brandani[2] and Paul A. Wright[1,*]

[1] *EaStCHEM School of Chemistry, University of St. Andrews, Purdie Building, North Haugh, St Andrews, Fife, KY16 9ST, UK*

[2] *School of Engineering, The University of Edinburgh, The King's Buildings, Edinburgh, EH9 3FB, UK*

[3] *Johnson Matthey Technology Centre, Chilton, PO Box 1, Belasis Avenue, Billingham, TS23 1LB, UK*

[4] *Diamond Light Source Ltd, Harwell Science and Innovation Campus, Didcot, Oxfordshire, OX11 0DE, UK*

Abstract

The adsorption of CO_2 on zeolite Li-Rho (unit cell composition $Li_{9.8}Al_{9.8}Si_{38.2}O_{96}$) has been investigated by the measurement of adsorption isotherms (273 – 300 K), breakthrough curves with a CO_2/CH_4/He mixture (308 K) and *in situ* synchrotron X-ray powder diffraction in CO_2 (298 K). The Rho framework distorts when in the Li-form to give a shape selective adsorbent for CO_2 over CH_4, although breakthrough curves reveal diffusional limitations. *In situ* synchrotron powder XRD follows the expansion of the Li-Rho unit cell upon adsorption, which remains single phase to a CO_2 pressure of *ca*. 0.6 bar. Partial cation exchange of Li-

Rho by Na^+ or Cs^+ gives two series of M,Li-Rho zeolites (M = Na, Cs). Where the occupancy of window sites (8R, D8R) between *lta* cages is less than 50%, hysteresis is not observed in CO_2 isotherms at 298 K. For $Cs_{1.8}Li_8$-Rho, which has a larger unit cell and a wider window than zeolite Li-Rho due to the presence of large Cs^+ cations in double 8-ring sites, breakthrough curves indicate faster CO_2 diffusion without significant loss of selectivity. We propose this control of adsorption kinetics of the flexible zeolite Rho via modification of cation content as a mechanism for cation controlled molecular sieving.

1. Introduction

The selective adsorption of CO_2 is important for a range of separation technologies, including purification of air,[1] natural gas and biogas upgrading[2-5] and carbon capture from pre- and post-combustion gas streams.[6] Small pore zeolites are promising sorbents for this purpose,[7,8] because their performance can be adjusted through control of their polarity, cage and window size, pore capacity and extra-framework cation content.[9-12] Commonly, the aluminosilicate framework of a zeolite is considered rigid, with a pore size derived from crystallographic measurements – values for which can be found in the 'Atlas of Zeolite Framework Types'[13] – so that its molecular sieving performance is determined by the location of charge-balancing cations. In zeolite A, for example, the effective window size can be modified by cation exchange with Na^+, K^+ or Ca^{2+} (Linde 4A, 3A and 5A, respectively, where 4A, etc. refers to the effective pore size in Å).[14-16] Recent computational studies have demonstrated that extra-framework cations can move in the presence of CO_2,[17] making cation gating effects possible.[18-24] In the postulated 'trapdoor' mechanism, cations occupying window sites permit the passage of molecules such as CO_2 or H_2O that interact strongly with cations but block the windows to molecules that interact more weakly (such as CH_4 or N_2). These 'trapdoor'

zeolites adsorb CO_2 from mixtures of CH_4 or N_2 with very high selectivity. Zeolites A[18,19] and chabazite[20,21] with particular cation compositions have been suggested to demonstrate such behaviour, as have certain forms of zeolite Rho[22-24] and structures related to Rho.[25,26]

In zeolite Rho,[27] large *lta* cages are linked by double 8-ring structural units, which act as windows and are also the favoured sites for large univalent cations such as Na^+, K^+ and Cs^+ (8-ring refers to a ring of 8 framework metal atoms and 8 oxygen atoms). These cations adopt sites in either single 8-rings or double eight-rings (represented as 8R or D8R sites in this work) depending on their ionic radius (Figure 1). Na-Rho with a framework Si/Al ratio of 3.9 has Na^+ cations in 8R sites in every double 8-ring window and yet still permits CO_2 uptake at low pressures while excluding CH_4.[23] However, the kinetics of adsorption and desorption in this Na-Rho are not fast enough for pressure swing adsorption applications, where timescales less than a few minutes are required. As a consequence, alternative approaches to high selectivity must be found that also permit rapid adsorption/desorption cycles. A kinetic separation mechanism based on pore size was suggested for a Cs,Na-Rho which gave good separation in breakthrough curves on a reasonable timescale (minutes) at relatively low CO_2 pressures, although additional cation gating effects cannot in that case be ruled out.[24] Certainly, kinetic separation of molecules of different dimensions on the basis of pore size has previously been shown to be possible for CO_2/CH_4 separation over carbon molecular sieves.[28]

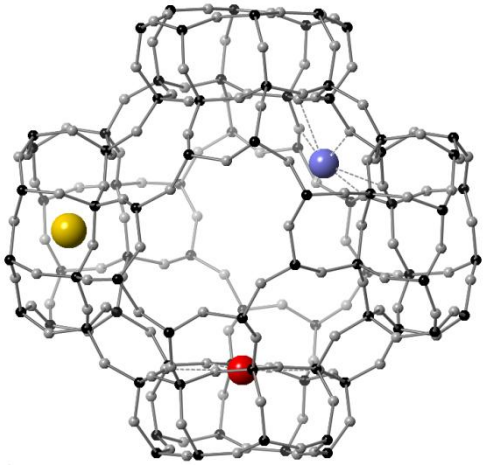

Figure 1. Cation sites in a cage of zeolite Rho. Double 8-ring site (D8R), yellow; single 8-ring site (8R), red; single 6-ring site (6R), blue.

All Rho materials referred to in this work have the same framework Si/Al ratio, 3.9, as those we have described previously,[22,23] unless stated otherwise. Unlike the other alkali metal cation forms of this zeolite Rho, the lithium form (Li-Rho) shows reversible CO_2 adsorption and desorption isotherms without hysteresis.[22] In Li-Rho the Li^+ cations (cation radius 0.70 Å) adopt 6-ring (6R) sites in the *lta* cages[22,29] in preference to 8R or D8R sites in the windows (Figure 1). As a consequence the majority of the windows in Li-Rho are left unblocked and CO_2 molecules can pass through these relatively unhindered. Percolation theory indicates that in cubic lattices (such as Rho) all internal space can be reached if the occupancy of windows by blocking cations is below ca. 50%.[30] Furthermore, only at a blocked window site fraction of ca. 2/3 does long range diffusivity through a cubic cage and window structure drop to approximately zero.[31] The presence of the small Li^+ cations in 6R sites has the effect of distorting the framework so that the 8-ring windows become strongly elliptical, with a crystallographic free diameter of 1.90 Å[22] (assuming a van der Waals radius for O of 1.35 Å[13]). We therefore expected these openings to be too narrow to allow the uptake of small hydrocarbon molecules such as methane which are larger than CO_2 with Lennard-Jones σ

3.73 Å and 2.98 Å, respectively.[32] Furthermore, we found that the presence of low fractional occupancies of alkali metal cations larger than Li^+ (e.g. $M^+ = Na^+, Cs^+$) in the window sites of mixed cation M,Li-Rho changed the unit cell size, and this was expected to modify adsorption selectivity and kinetics.

We aimed to control the molecular sieving behaviour of Li-Rho in separations of CO_2 from CH_4 and so we prepared series of mixed cation Na,Li- and Cs,Li-Rho materials and investigated their selectivity and kinetics of adsorption from CO_2/CH_4 mixtures typical of certain natural gases. We report the CO_2 adsorption behaviour of Li- and M,Li-Rho materials, including adsorption isotherms and CO_2/CH_4 breakthrough curves, and relate it to their structural response, as determined by analysis of synchrotron X-ray powder diffraction data measured under CO_2 gas pressures.

2. Experimental

2.1 Preparation and Characterisation of Dehydrated Li- and M,Li-Rho materials

Zeolite Rho with a Si/Al ratio of 3.9 was synthesised in the Na,Cs-form in the presence of the crown ether, 18-crown-6.[33] The organic was removed by calcination and Li-Rho and mixed M,Li-forms of zeolite Rho(3.9) (M ≡ Na or Cs) were prepared via sequential aqueous cation exchange steps and analysed by a mixture of EDX and atomic adsorption as described in the Supporting Information. In addition, a sample of Li-Rho with a framework Si/Al of 3.2 was prepared via a crown ether-free preparation adapted from the literature[34] followed by extensive lithium exchange as described in the Supporting Information (described here as Rho(3.2)). The compositions of specific mixed cation samples in this work, determined by a combination of chemical analysis and Rietveld refinement of diffraction data, are given in the form M_xLi-Rho, where M = Na or Cs, *x* is the number of M^+ cations per unit cell, and the

remaining framework charge per unit cell is balanced by Li^+ cations. The total negative framework charge per unit cell of Rho(3.9) is -9.8. More generally, we use M,Li-Rho to denote mixed cation zeolites.

Powder X-ray diffraction (PXRD) patterns of all Rho samples were measured in dehydrated form. Samples were loaded into 0.7 mm quartz glass capillaries and heated for 16 h at 623 K under a vacuum of 10^{-7} bar, before being sealed under vacuum and run in Debye-Scherrer geometry on a Stoe STAD i/p diffractometer using Cu K_α X-rays (1.54056 Å).

2.2 Adsorption Isotherms and In Situ PXRD Measurements CO_2 adsorption isotherms for all samples were measured volumetrically at 298 K from 0 to 1 bar, using equilibration times of up to two hours. These measurement conditions give reversible isotherms where diffusion is relatively fast but give marked hysteresis loops when adsorption is diffusion rate-limited. Such hysteresis loops have previously been described for other compositions of zeolite Rho.[22,35] In addition, for Li-Rho, $Na_{2.1}$Li-Rho and $Cs_{1.8}$Li-Rho, series of adsorption isotherms were collected at 273, 278, 283 and 293 K using a Micromeritics 2020 porosimeter. For these series, the isosteric heats of adsorption were calculated by interpolation of the uptake/pressure data and plots of ln$p$ vs. 1/T at fixed uptakes. In addition, methane adsorption isotherms were measured volumetrically on selected samples using the Micromeritics instrument at 298 K, and ethane adsorption isotherms were measured on Li-Rho and H-Rho[22] at 298 K on a custom-built laboratory glass line.

To investigate the structural basis of the reversibility (or otherwise) of CO_2 adsorption on Rho, in situ synchrotron X-ray powder diffraction at beamline I11 of the Diamond Light Source[36,37] was performed on Li-Rho and $Cs_{2.5}$Li-Rho samples that showed rapid and reversible CO_2 uptake and a $Na_{6.2}$Li-Rho sample that adsorbed CO_2 more slowly and demonstrated hysteresis. The samples were each loaded in a 0.7 mm quartz glass capillary,

held in place by a quartz wool plug and attached to a goniometer head attached to a gas handling system. The samples were dehydrated at 500 K for 2 h (with additional treatment by hot air gun at 573 K for *ca*. 10 min) under a vacuum of 10^{-8} bar, prior to the stepwise addition of CO_2 up to 10 bar, after which the CO_2 pressure was reduced stepwise. For those samples that showed no hysteresis, diffraction patterns were taken every 3 minutes until there was little visual change, whereas for $Na_{6.2}$Li-Rho a diffraction pattern was taken 15 min after each increase (or decrease) in CO_2 pressure. Diffraction patterns were measured for 5 or 10 s per pattern using monochromated X-rays (λ = 0.826956 or 0.826163 Å) and a MythenII position sensitive detector.[37]

2.3 Crystallography Rietveld structure refinements of zeolite Rho materials in the dehydrated state and with adsorbed CO_2 were carried out using the GSAS suite of programs.[38] For the dehydrated Rho materials determined by refinement against laboratory PXRD data, the structure of Li-Rho (space group *I*-43*m*) reported previously[22] was used as a starting model. Restraints were applied to Si,Al-O and tetrahedral O-O distances (1.63 and 2.66 Å, respectively) for these and all synchrotron PXRD refinements. Background was fitted by a 36 term shifted Chebyshev function and peak profiles matched by a Pseudo-Voigt profile function. In M,Li-Rho samples, Na^+ or Cs^+ cations were located by refining electron density at the 8R and D8R sites they are known to occupy in the dehydrated Rho structure (Na^+ preferentially at 8R, Cs^+ at D8R). Li^+ cation occupancies were then fixed in 6R sites knowing the chemical composition and assuming Li^+ cations preferentially adopt 6R sites.

A similar approach was adopted for refinements of Li-Rho, $Na_{6.2}$Li-Rho and $Cs_{2.5}$Li-Rho samples measured by PXRD during CO_2 adsorption at beamline I11 at the Diamond Light Source. The compositions given here for M,Li-Rho samples are in terms of the Na^+ or Cs^+

cations whose occupancies were established by structural refinement: Li^+ cations make up the residual cation content. In the dehydrated Li- and $Cs_{2.5}$Li-Rho samples, cation occupancies at sites occupied by Li^+ (6R, 8R) and Cs^+ (D8R) were obtained (capping Li^+ in 6R sites at full occupancy), whereas for the $Na_{6.2}$Li-Rho, Na^+ cations were refined in the 8R sites and the remaining Na^+ and Li^+ placed together at the 6R sites.

Different strategies were used to refine the structures with adsorbed CO_2. For Li-Rho and $Na_{6.2}$Li-Rho, two sites for CO_2 (with constrained linear molecular geometry) were located as described previously for Na-Rho, and their occupancies refined. Although Li^+ cation positions and occupancies could be refined in the dehydrated forms with no CO_2, this was not possible for Rho zeolites with adsorbed CO_2. In these cases the refinements began with the dehydrated forms and then structures with increasing adsorbed CO_2 were refined sequentially. Cation occupancies and positions were held at their last refined values or moved to chemically sensible positions and kept fixed there, according to a model where Li^+ cations favour 6R sites in aluminosilicate zeolite Rho. For $Cs_{2.5}$Li-Rho the different location of Cs^+ prompted us to detect extra-framework scattering by different Fourier analysis, and refine this as isolated O atoms of CO_2 molecules. Three sites for O atoms were located: their position and occupancy were refined. The weak X-ray scattering factor of Li^+ and disorder of CO_2 makes precise verification of Li, C and O positions by powder X-ray diffraction in all these structures highly challenging, and so they are presented as structural models which enable determination of framework geometry and Cs^+ positions. Only single phase materials were structurally refined. Details of all these refinements are given in the Supporting Information (Tables S2.1 - S2.11, Figures S2.1 - S2.19, also in the cif files).

2.4 Breakthrough Curve Analysis[39-45] CO_2/CH_4 breakthrough curves were measured at 308 K for gases of composition 5% CO_2 / 40% CH_4 / 55% He, where the CO_2 and CH_4 levels were taken as representative of a CO_2-containing natural gas. Li-Rho, $Na_{2.1}$Li-Rho and $Cs_{1.8}$Li-Rho were examined. In these experiments, a special "elongated" version of the Zero Length Column (E-ZLC) was used. The E-ZLC consists of a Swagelok 1/8" bulkhead union with an internal diameter of 2.286 mm and a length of 25.9 mm. As a result the columns can hold up to 5× the amount of sample that is normally used in a typical ZLC experiment, allowing a clear identification of the separation performances. Apart from the extended column, the experimental apparatus used for this study is the same as the Zero Length Column (ZLC) set-up described in previous work.[39,40] In order to minimise the pressure drop across the column, the samples were made as binderless pellet fragments *ca.* 2 mm in dimensions: 43 mg for Li-Rho, 46.3 mg for $Na_{2.1}$Li-Rho and 53.9 mg for $Cs_{1.8}$Li-Rho.

Multi-component breakthrough experiments were carried out at a total pressure of 1 bar, 308 K and different flowrates (1, 2 and 5 ml min^{-1}). In addition to the multicomponent experiments, single component CH_4 breakthrough experiments (40% CH_4 in He), were carried out at the same conditions to verify the CH_4 uptake on the samples under similar conditions. Prior to the experiments, the samples were regenerated overnight at 623 K under He flow. The experiment consists in equilibrating the sample to a constant flowrate of the feed mixture. Once equilibrium is reached the flow is switched to pure He and the desorption starts. During the entire length of the experiment all the components of the feed mixture are followed using a Dycor Ametek Benchtop quadrupole mass spectrometer (MS) connected at the outlet of the column.

To enable analysis of the results, blank runs were also carried out. These consist of repeating the breakthrough experiments under the same conditions as described above, but without adsorbent. In this case the column is filled with 2 mm glass beads to give a pressure drop and

void fraction close to that observed in the presence of the samples. This allows the dead volume and the intrinsic kinetics of the system to be measured when no adsorption occurs. The experimental breakthrough curves are analysed using CySim, the in-house adsorption process simulator.[41] The simulator, originally developed for the simulation of the dual-piston PSA system[42] was extended to the simulation of general adsorption cycles.[43,44] and more recently to the analysis of ZLC experiments.[44] CySim incudes different modular units, including adsorption columns, valves and splitters, which can be combined to simulate the desired adsorption process. The simulator includes accurate multicomponent mass and energy balances which allow the adsorption column dynamics to be described, taking into account variable flowrates and nonlinearities in the system. For this study the system simulated is the same as that used previously for modelling ZLC measurements, with the difference that the dimensions of the columns correspond to those of the E-ZLC.

3. Results and Discussion

3.1 Structure of Dehydrated Li,M-Rho Table 1 lists the zeolite Rho materials prepared and characterised in this work, giving the composition, the unit cell parameter in the dehydrated state, and the cation location determined by Rietveld refinement. In the structure of dehydrated Li-Rho, reported previously, it was possible to locate Li^+ cations in the 6R sites, but even if full occupancy of those sites is assumed, that would leave 1.8 Li^+ cations per unit cell elsewhere. Notably, in Li-Rho(3.2), the structure of which is refined in this work for the first time, Li^+ is observed in 6R and 8R sites, preferentially in the former (Tables S2.1, S2.4, Figure S2.7). The dehydrated form of this Li-Rho(3.2) has a strongly reduced unit cell (14.1715(2) Å) when dehydrated.

In M,Li-Rho materials, Na^+ and Cs^+ cations are located in 8R and D8R window sites, respectively, when present at <6 per unit cell. In this work, the Na^+ or Cs^+ occupancies are refined and the Li^+, which is very difficult to locate accurately by XRD was placed in 6R sites as a plausible model. In samples with more than *ca.* 6 Na^+ per unit cell, some Na^+ cations are located in 6R sites. The presence of Na^+ or particularly Cs^+ in window sites in M,Li-Rho zeolites results in an increase in unit cell size compared to Li-Rho. This effect is small for Na_xLi-Rho (14.3331(3) Å for $Na_{2.1}$Li-Rho *cf* 14.2448(2) Å for Li-Rho) but larger for Cs_xLi-Rho (14.4691(2)Å for 2.8 Cs^+ cations).

Table 1. Compositions and unit cell parameters for Li-, Na,Li- and Cs,Li-Rho samples analysed. Cation site occupancies determined by Rietveld refinement.

Unit cell compositions (estimated)	Unit cell parameter (Å)	Number of cations in D8R	Number of cations in 8R	Number of cations in 6R (Li placed unless refined*)	Number of Li cations (AAS)
$Li_{9.8}Al_{9.8}Si_{38.2}O_{96}$	14.2448(2)	-	1.8 Li	8.0 Li	9.8
$Li_{11.4}Al_{11.4}Si_{36.6}O_{96}$	14.1715(5)	-	2.3 Li*	7.2 Li*	-
$Na_{2.1}Li_{7.7}Al_{9.8}Si_{38.2}O_{96}$	14.3017(1)	-	2.1 Na	7.7 Li	7.4
$Na_{4.3}Li_{5.4}Al_{9.8}Si_{38.2}O_{96}$	14.3176(2)	-	4.3 Na	5.4 Li	5.5
$Na_{8.0}Li_{1.8}Al_{9.8}Si_{38.2}O_{96}$	14.3331(3)	-	5.0 Na	1.8 Li, 3.0 Na	2.4
$Cs_{0.8}Li_{9.0}Al_{9.8}Si_{38.2}O_{96}$	14.3559(6)	0.8 Cs	-	8 Li	7.6
$Cs_{1.8}Li_{8.0}Al_{9.8}Si_{38.2}O_{96}$	14.4113(3)	1.8 Cs	-	8 Li	7.0
$Cs_{2.8}Li_{7}Al_{9.8}Si_{38.2}O_{96}$	14.4691(2)	2.8 Cs	-	7.2 Li	6.4
$Na_{6.2}Li_{3.6}Al_{9.8}Si_{38.2}O_{96}$[a]	14.3384(3)	-	5.4 (Na)	3.0 (Li) 0.8 (Na)	3.5
$Cs_{2.5}Li_{7.0}Al_{9.8}Si_{38.2}O_{96}$[a]	14.4789(1)	2.5 (Cs)	-	7.0 (Li)	7.1

[a] Examined using diffraction using synchrotron X-radiation. All other refinements with laboratory PXRD.

3.2 Adsorption on Li-Rho Li-Rho was previously found to adsorb CO_2 with a high uptake (5 mmol g^{-1} at 1 bar at 298 K) and without hysteresis, even at the relatively short equilibration times used in the screening experiments.[22] In this work, adsorption isotherms were measured between 273 K and 293 K and the isosteric heat of adsorption was determined as a function of uptake (Figure 2). The heat of adsorption was estimated to increase from *ca.* 25 kJ mol^{-1} to 36 kJ mol^{-1} as the CO_2 uptake increases from 0 to 1 mmol g^{-1}, and then stays at approximately this value as the uptake increases to 4 mmol g^{-1}, decreasing slightly thereafter.

Li-Rho did not adsorb significant amounts of CH_4 at 308 K (as seen from CH_4 breakthrough desorption curves (see below) or C_2H_6 at 293 K (Figure S3.1).

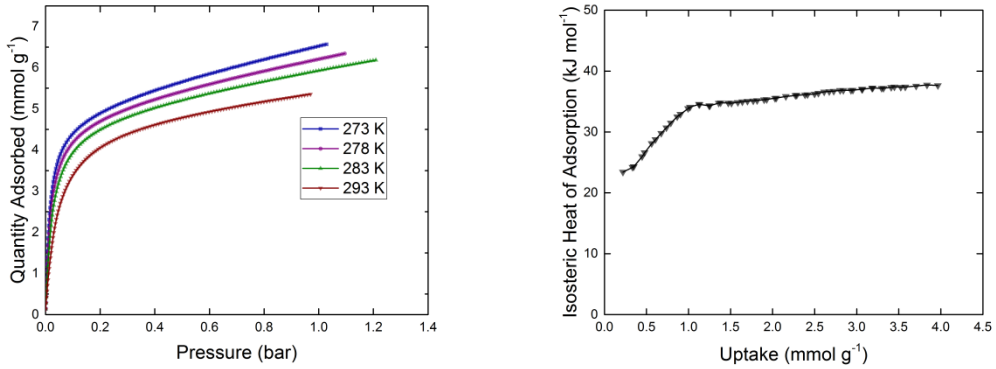

Figure 2. (Left) CO_2 adsorption isotherms on Li-Rho at 273 - 293 K and (right) isosteric heats of adsorption of CO_2 (±1 - 1.5 kJ mol^{-1}) on Li-Rho as a function of uptake.

The effect of Li^+ in 6R sites in Rho is to distort the framework, which adapts to coordinate the small Li^+ cations more closely, and consequently to reduce the size of the opening to a crystallographic minimum free diameter of 1.90 Å.[22] This does not prevent the diffusion of CO_2 (2.98 Å[32]). Notably, Li-Rho(3.2) does show significant hysteresis in its CO_2 adsorption isotherm measured at 298 K under the same conditions (Figure S3.2). We speculate that this arises because at the higher Li^+ occupancies in the 8R sites of this material (expected to be >50% given its composition) some motion of the Li^+ cations is required for uptake in this material.

In situ synchrotron X-ray powder diffraction showed that the unit cell of the dehydrated form of Li-Rho in these experiments (14.3446(1) Å) is slightly larger than that measured for samples dehydrated for many hours at 623 K in the laboratory. This is a result of incomplete water removal under the limited heating time and facilities available at the synchrotron (500 K was the highest temperature available for prolonged *in situ* heating of capillaries).

Nevertheless, the unit cell for the Li-Rho determined by synchrotron data is much smaller than that of the fully hydrated material, indicating most of the water has been removed. Li^+ cations are located in 6R sites and in the distorted 8R sites, although the occupancy is difficult to determine exactly given the low scattering of Li^+ and the presence of some water.

Upon CO_2 adsorption at 298 K, *in situ* PXRD (Figure 3) showed that Li-Rho remained a single phase as the pressure was increased from 0 – 0.62 bar, and the unit cell increased gradually from 14.3446(1) Å in the dehydrated, evacuated, form up to 14.5875(3) Å at a CO_2 pressure of 0.888 bar (Figure 4, Table S2.6). At this pressure, a small amount of a second phase with a slightly larger unit cell parameter was observed, the amount of which increased until the sample again became single phase at 9 bar (a = 14.7561(8) Å). Reducing the CO_2 pressure results in a reduction of the unit cell, as the CO_2 is reversibly desorbed. Full evacuation regenerates a single phase, with a slightly larger unit cell than the dehydrated Li-Rho, suggesting that after 10 minutes some adsorbed CO_2 remained. Nevertheless, the PXRD data is consistent with adsorption and corresponding structural 'breathing' that is nearly reversible on the 10 min timescale of each adsorption step, which is consistent with the reversible CO_2 isotherm.

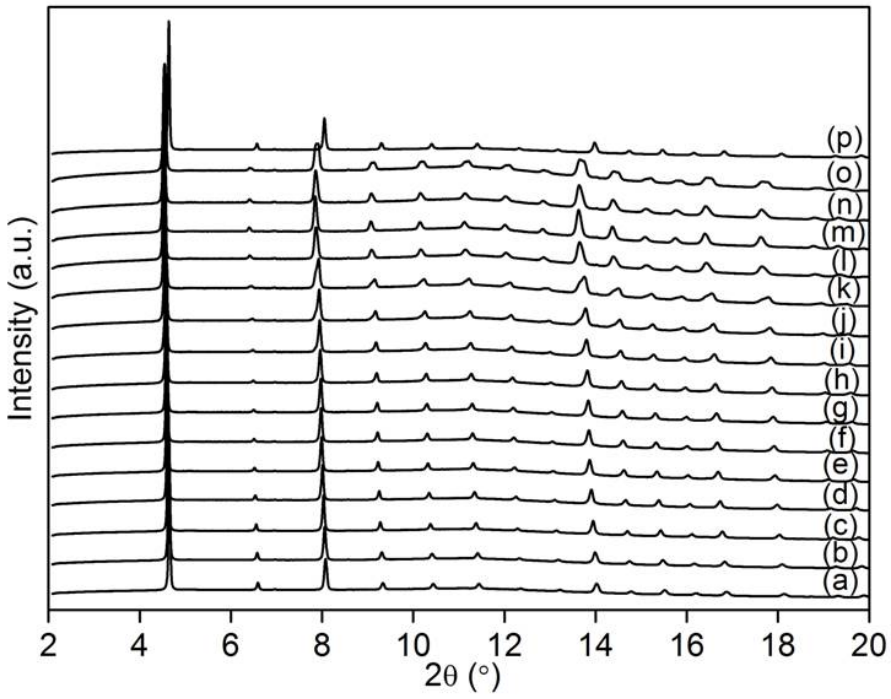

Figure 3. PXRD of Li-Rho (a) dehydrated and measured with CO_2 adsorbed at different pressures (in bar): (b) 0.052, (c) 0.097, (d) 0.150, (e) 0.220, (f) 0.287, (g) 0.387, (h) 0.617, (i) 0.888, (j) 1.174, (k) 2.530, (l) 4.900, (m) 9.000, (n) 4.250, (o) 1.400 and (p) evacuated.

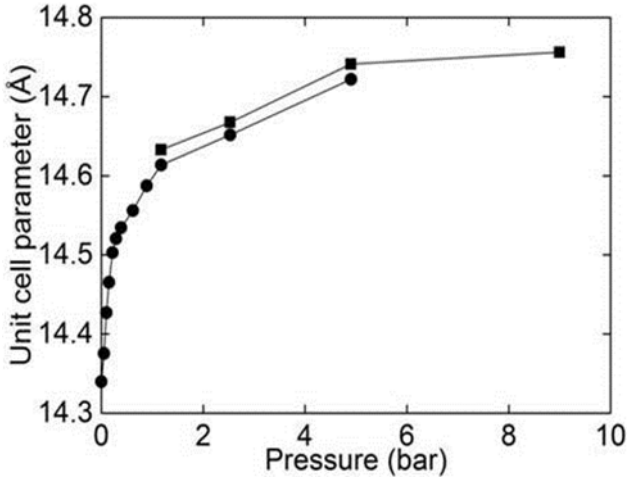

Figure 4. Unit cell parameter of Li-Rho upon adsorption of CO_2 (equilibration time 10 min). Two Li-Rho phases with slightly different unit cell parameters (represented by circles and squares) co-existed from 1 - 5 bar.

Rietveld refinement of the Li-Rho framework structure from these *in situ* experiments shows that the unit cell expansion is associated with a decrease of the ellipticity of the 8R windows.[46] As the CO_2 pressure is increased from 0 to 0.617 bar, the minimum free diameter of the window increases from 2.20 Å to 2.86 Å. We interpret this change in the framework structure as resulting from the increased coordination of Li^+ cations by CO_2. These therefore exert a decreased tendency to distort the structure away from its high symmetry form. For comparison, the unit cell of hydrated forms of Rho, in which the cations are fully hydrated and their effective charge density reduced, expands so that a = 15.0 Å. The increase in heat of adsorption of CO_2 on Li-Rho with increasing uptake, particularly up to *ca*. 1 mmol g^{-1} (Figure 2b) is opposite to what is usually observed for cationic zeolites, where the first molecules to be adsorbed are located at the most strongly adsorbing sites.[47] We speculate that the lower initial heats might be associated with the energy that must be expended to allow Li^+ cations to move away from the framework to coordinate to CO_2 molecules, although the unit cell measurements indicate that expansion continues to pressures corresponding to uptakes of several mmol g^{-1}. Detailed studies are required to investigate this observation further.

The adsorption data indicate that the CO_2 molecules (2.98 Å[32]) can pass through the empty window sites and equilibrium is reached on a time scale of tens of minutes in these experiments, but small alkane molecules (e.g. CH_4, 3.73 Å[32]) are too large to be adsorbed (Figure S3.1). The situation is very different for adsorption on H-Rho, which has circular 8-ring windows with a free diameter of 4 Å, readily allowing ethane to be adsorbed (2.5 mmol g^{-1} of C_2H_6 at 293 K at 1 bar (Figure S3.1)). The effect of the Li^+ cations is to control the window diameter by the electrostatic effect they exert on the framework in both 6R and (partially occupied) 8R sites (Figure 5).

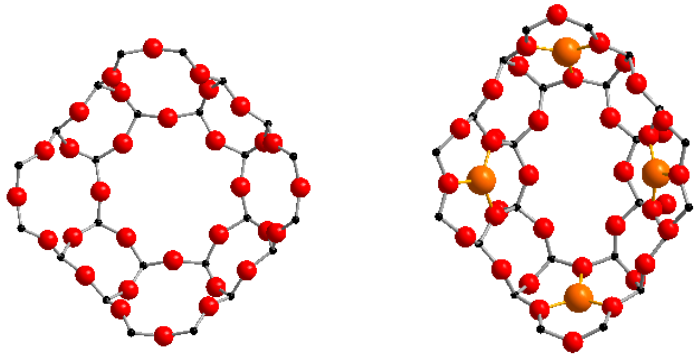

Figure 5. Views of part of the structures of (left) H-Rho and (right) Li-Rho, both in the dehydrated form, showing the change in shape of the 8-ring window (Si atoms, black; O atoms, red; Li^+ cations, orange).

This is a type of cation controlled molecular sieving where the cations do not control the pore size by partial blocking, but rather by controlling the extent of framework distortion in a flexible zeolite. The magnitude of this effect will depend on the number and type of cations present and so is readily tunable. However, in the presence of a strongly coordinating adsorbate, the window size will also depend on the level of uptake of this component, so true measures of the separation over these zeolites require mixed component adsorption to be examined.

Mixed component CO_2/CH_4 breakthrough and desorption curves for Li-Rho are shown in Figure 6. In order to compare the different samples the curves are plotted as dimensionless concentration versus the volume of gas eluted (flowrate × time) normalised against the mass of adsorbent. The plot of the adsorption branch of the breakthrough experiment clearly shows that even in a CH_4-rich environment the Li-Rho can achieve separation between CH_4 and CO_2. The difference in the breakthrough time indicates a significant amount of CO_2 adsorbed with practically no CH_4 adsorption. This becomes even more obvious from the analysis of the

desorption branch, in which the CH_4 curve is not readily distinguishable from the decrease in signal from a breakthrough experiment measured without zeolite, giving the same response of a system without adsorption. The amount of CO_2 adsorbed on Li-Rho calculated from the simulations is 1.28 mmol g^{-1} while the CH_4 desorption curve overlaps with the blank of the system, indicating no appreciable adsorption of CH_4. This shows that the Li-Rho is a highly selective adsorbent under these conditions (essentially infinite selectivity for CO_2/CH_4). However, the relatively diffuse front of CO_2 from the column suggests that the CO_2 molecules experience some mass transfer limitations.

The results from matching the CySim simulations to the desorption curve yield a diffusional time constant, R^2/D, of 28 min. Figure 6b shows the comparison of the experimental and predicted curves for this sample. In addition, a single component CH_4 breakthrough experiment (40% CH_4 in He) was carried out to investigate CH_4 adsorption in the absence of CO_2. For Li-Rho, the experiment suggests an uptake < 0.18 mmol g^{-1}, but the shape of the desorption curve, which nearly overlaps the blank, indicates that this uptake is likely to result from adsorption at the external surface of the sample rather than within the pores.

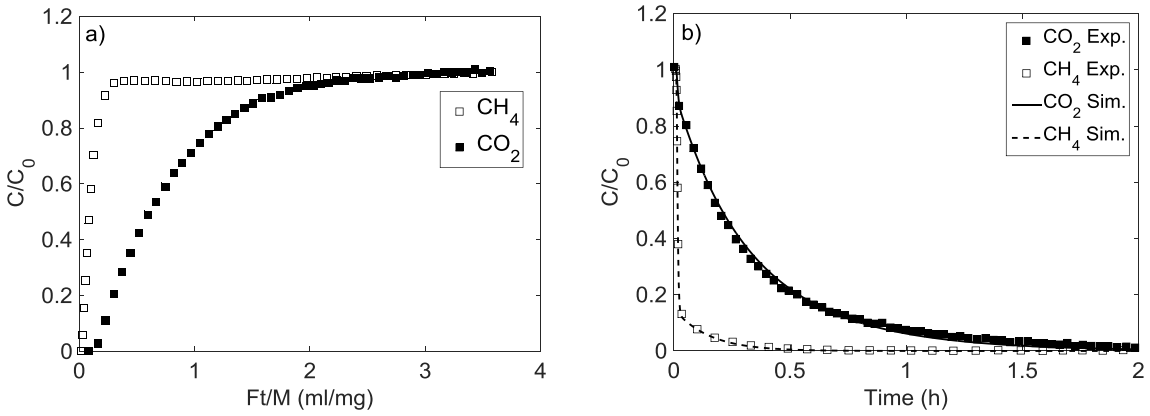

Figure 6. Experimental multicomponent breakthrough curves (a) and subsequent desorption curves (b) for Li-Rho. Feed conditions CO_2/CH_4/He = 5/40/55, P = 1 bar, T = 308 K, followed by a switch to He flow.

In light of the kinetic limitations on CO_2 diffusion through Li-Rho, we examined the effect of partially exchanging Li^+ by Na^+ and Cs^+, which occupy window sites preferentially. The aim was to increase the size of the 8-ring windows while leaving enough free for percolation, and in this way to allow fast CO_2 uptake while retaining the molecular sieving behaviour.

3.3 Adsorption on Mixed Cation Na,Li-Rho Zeolites A series of mixed Na,Li-forms of Rho was prepared, of general unit cell formula $Na_xLi_{9.8-x}Al_{9.8}Si_{38.2}O_{96}$, with x = 0 – 9.8. The unit cell of the dehydrated forms of the zeolites determined by Rietveld refinement against the laboratory PXRD data increased with increasing Na^+ content (Table 1): Li-Rho (14.2448(2) Å), $Na_{2.1}$Li-Rho (14.3017(1) Å), $Na_{4.3}$Li-Rho (14.3176(2) Å) and $Na_{6.3}$Li-Rho (14.3331(3) Å). The CO_2 adsorption isotherms on this Na,Li-Rho series are given in Figure 7.

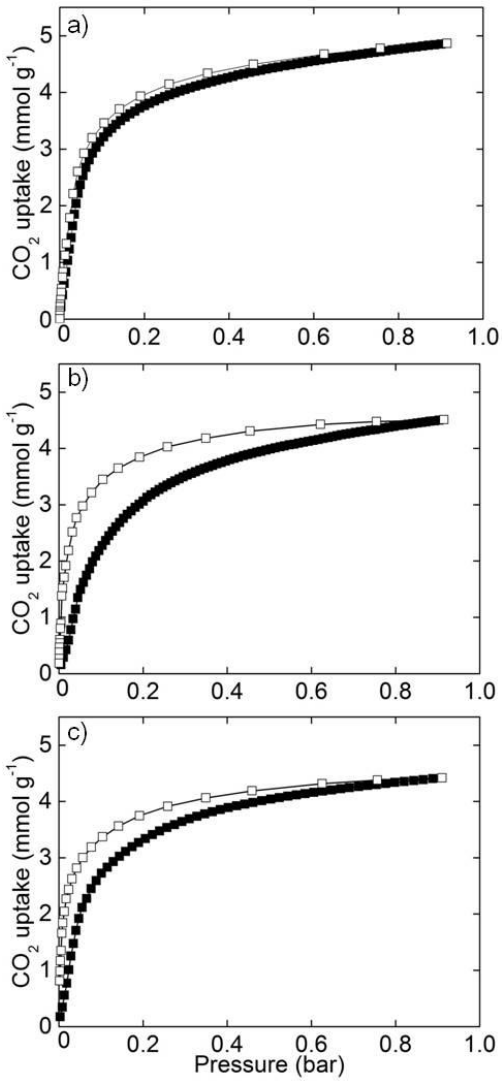

Figure 7. CO_2 isotherms at 298 K (adsorption, closed squares, and desorption, open squares) for the Na,Li-Rho series: (a) $Na_{2.1}$Li-Rho, (b) $Na_{4.3}$Li-Rho and (c) $Na_{6.3}$Li-Rho.

At low Na^+ loadings (e.g. x = 2.1) the measured adsorption/desorption isotherms show little hysteresis, and the behaviour is very similar to that of the pure Li-Rho. A series of CO_2 isotherms at different temperatures was measured on the $Na_{2.1}$Li-Rho sample and the isosteric heats of adsorption calculated (Figure S4.1). The initial heats of adsorption are not markedly lower in the way that is observed for Li-Rho and over the whole range the heats are slightly higher (35 – 41 kJ mol^{-1}). Measurement of the CH_4 uptake from the single component breakthrough at 1 bar suggested an uptake of < 0.2 mmol g^{-1}, while a single component

adsorption isotherm at 298 K (Figure S4.2) indicates an uptake of only 0.05 mmol g^{-1} at 0.4 bar, indicating that the pore size is too small to take up methane.

The breakthrough curve over $Na_{2.1}$Li-Rho for the CO_2/CH_4/He mixture (Figure 8) is similar to that of Li-Rho, although the CO_2 breakthrough is a little sharper, suggesting that the slightly larger initial window size of dehydrated $Na_{2.1}$Li-Rho compared to that of Li-Rho (14.3017(3) Å vs. 14.2448(2) Å) allows slightly faster CO_2 diffusion. From the desorption curve (Figure 8, including simulated curves) a CO_2 uptake of 1.37 mmol g^{-1} was calculated.

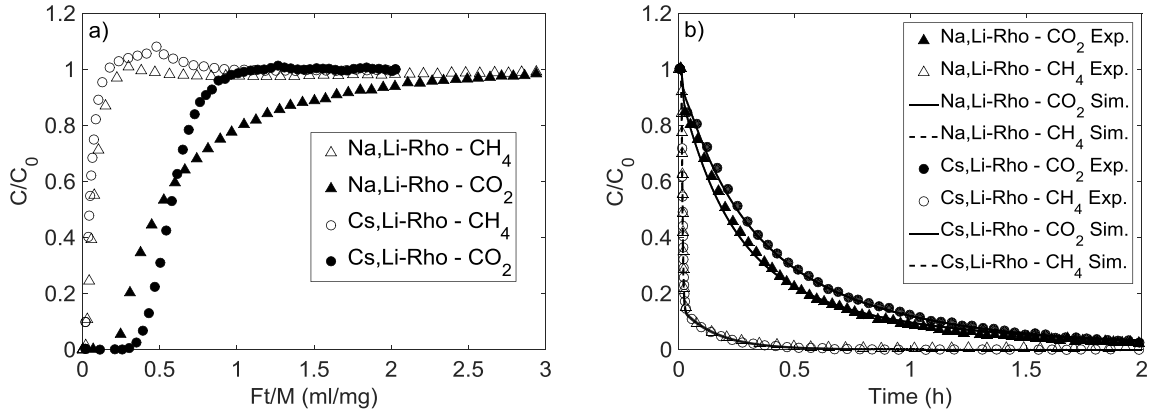

Figure 8. Breakthrough curves (a) and subsequent desorption curves (b) for $Na_{2.1}$Li-Rho and $Cs_{1.8}$Li-Rho. Feed conditions CO_2/CH_4/He = 5/40/55, P = 1 bar, T = 308 K, followed by switching to He.

The equilibrium selectivity of CO_2/CH_4 was determined from the desorption branch of the breakthrough curves. This allows extraction of the adsorption parameters after the system has reached equilibrium, thereby reducing the uncertainties due to the presence of the roll-up during the adsorption. The final equilibrium selectivity is high, >200, while the desorption

kinetics are slightly faster than those of the Li-Rho, with a diffusional time constant of 21 min, suggesting that the pore size of the $Na_{2.1}$Li-Rho is slightly larger than that of Li-Rho.

At higher Na^+ contents in the Na,Li-Rho series the adsorption/desorption hysteresis becomes much more significant (Figure 7), and is even larger than that for the pure Na-Rho observed previously.[22,23] The slow kinetics observed for the Na-rich end of the solid solution series can be attributed to the presence of Na^+ cations in 8R window sites at levels that require access to cages in the structure via occupied windows, with resulting need for cation movement. *In situ* synchrotron PXRD (Figure S2.11, also Table S2.8) of a sample of composition $Na_{6.2}$Li-Rho shows that the dehydrated form has a unit cell parameter of 14.3384(1) Å, which only slightly increases to 14.3513(2) Å with the introduction of 0.1 bar CO_2. At 0.2 bar CO_2 a second Rho phase, with a larger unit cell, can just be identified. The fraction of the larger unit cell phase of Rho increases continuously as p_{CO2} is increased (to 0.3 and 0.4 bar) until at 0.5 bar the larger unit cell phase is the major phase. By 10 bar all of the Rho is in the larger unit cell form, with unit cell parameter ca. 14.6139(3) Å (Figure S2.11). The structures at 0 and 0.1 bar CO_2 were refined assuming CO_2 adopts two sites coordinated to 8R (Na^+) and 6R (Na^+, Li^+) cations. The presence of two different Rho phases over a wide range of p_{CO2} is very different from what is seen with Li-Rho. This is a consequence of the slow kinetics of the CO_2 adsorption process, which must require cation movement because of the high occupancy of the 8R window sites by Na^+. As a result, equilibrium is not achieved. The slower uptake in this material compared to the fully Na^+-exchanged form is likely to be because the presence of smaller Li^+ cations in the 6R sites rather than Na^+ results in a stronger distortion of the framework, a smaller unit cell and a more elliptical 8-ring, which results in the Na^+ cation being bound more strongly. This would then make the motion required of the Na^+ cation to permit CO_2 adsorption more difficult. Most significantly, this examination of CO_2 adsorption on $Na_{6.2}$Li-Rho illustrates the much slower kinetics of the adsorption requiring Na^+ cation

motion compared to those of M,L-Rho, where there is a lower than 50% occupancy of windows by cations.

3.4 Adsorption on Cs,Li-Rho We reasoned that if the presence of a fractional occupancy of Na^+ cations of *ca* 1/3 in the 8R sites of Na,Li-Rho could modify the diffusion rate of CO_2, the inclusion of larger Cs^+ cations would have a stronger effect. Fully-exchanged Cs-Rho admits almost no CO_2 up to 1 bar, because the Cs^+ cations occupy all D8R window sites and do not readily move to allow CO_2 passage.[23] A series of Cs,Li-Rho samples was therefore prepared with 0.8, 1.8 and 2.8 Cs^+ cations per unit cell and their CO_2 adsorption isotherms at 298 K were measured (Figure 9). Rietveld refinement indicated that in the fully dehydrated form these had significantly larger unit cell parameters than the Li-form (14.3559(6) Å, 14.4113(3) Å and 14.4691(2) Å, respectively, compared with 14.2448(2) Å). In each case, the Cs^+ cations occupy D8R sites in the dehydrated solids (Table 1). The minimum free diameter of the elliptical 8R windows increases from 1.90 Å in Li-Rho to 2.38 Å in $Cs_{2.8}$Li-Rho. In these materials, with Cs^+ in D8R sites, the uptake remained high for the lower Cs^+ cation contents (which permit percolation through empty windows) but decreased slightly for the highest Cs^+ content. Adsorption isotherms showed little hysteresis for these samples (Figure 9).

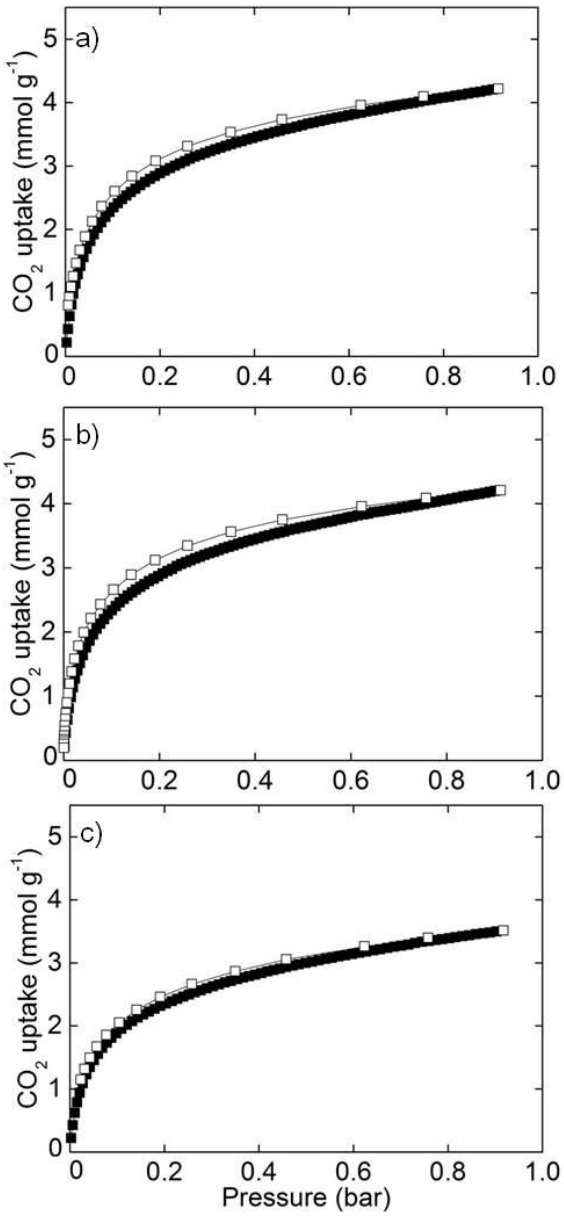

Figure 9. CO_2 isotherms at 298 K (adsorption, closed squares, and desorption, open squares) for the Cs,Li-series: (a) $Cs_{0.8}$Li-Rho, (b) $Cs_{1.8}$Li-Rho and (c) $Cs_{2.8}$Li-Rho.

$Cs_{1.8}$Li-Rho was examined by breakthrough curve analysis. The breakthrough curve using the same CH_4/CO_2/He mixture and flow-rates as for the other samples indicates a later breakthrough of CO_2, indicating a better dynamic separation (Figure 8). Also, the CH_4 signal indicates a roll-up feature suggesting that the zeolite may adsorb some CH_4 initially, which is displaced by CO_2. The shape of the adsorption curve from Figure 8 shows faster kinetics

relative to the other two samples: the time constant is estimated to be *ca*. 8.3 min. CH_4 uptake at 308 K from the single component CH_4 breakthrough experiment is measured to be < 0.1 mmol g^{-1}, while volumetric adsorption measurements (Figure S5.1) suggest an uptake at 298 K and 0.4 bar of 0.06 mmol g^{-1}, in each case indicating no significant uptake.

To understand the breakthrough curve behaviour a sample of Cs,Li-Rho was prepared with a similar composition, containing 2.5 Cs^+ cations per unit cell. This was then examined for CO_2 adsorption from 273 to 293 K and the isosteric heats calculated (Figure S5.2). The isosteric heat was found to be approximately constant at 37 kJ mol^{-1} up to an uptake of 3.5 mmol g^{-1}, decreasing thereafter to 32 kJ mol^{-1} at 5 mmol g^{-1}. A closer examination was then made of structural changes of this $Cs_{2.5}$Li-Rho sample upon CO_2 adsorption, by synchrotron X-ray powder diffraction (Figure S2.16, Figure 10; Table S2.10).

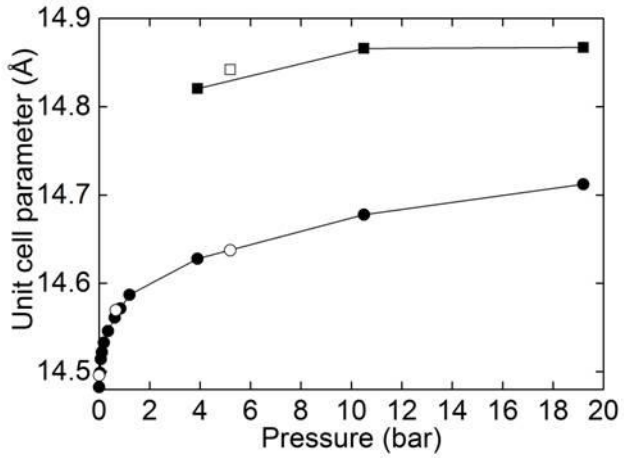

Figure 10. Unit cell parameters of $Cs_{2.5}$Li-Rho during adsorption and desorption of CO_2. showing two phases at higher pressure (Filled symbols, adsorption; empty symbols, desorption).

The unit cell of the dehydrated sample was 14.4789(8) Å. Upon adsorption at 293 K, CO_2 uptake occurred rapidly, and the $Cs_{2.5}$Li-Rho remained a single phase up to 1.2 bar, with the unit cell increasing only slightly to 14.5847(8) Å, less than is the case for the Li-Rho (Figures 10 and 11). Above this pressure a second phase appears and two phases co-exist up to 19 bar. Removal of pressure results in a reversible structural change as the CO_2 desorbs. Rietveld refinement of single phase structures (up to 1.2 bar) shows that the Cs^+ cations remain within the D8R sites at these adsorbate pressures (Tables S2.10, S2.11) and that the minimum free diameter of the elliptical 8-ring windows increases from 2.40 Å to 2.65 Å.

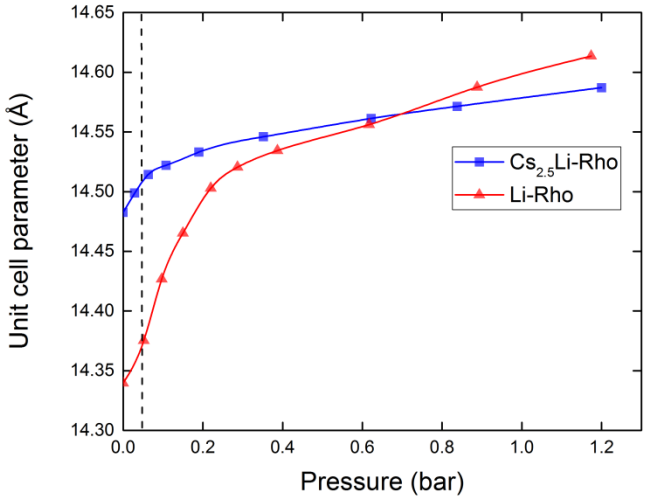

Figure 11. Comparison of the variation of the unit cell parameter of Li-Rho (red triangles) and $Cs_{2.5}$Li-Rho (blue squares) during adsorption of CO_2 from 0 – 1.25 bar at 295 K, as measured by synchrotron X-radiation. The partial pressure of CO_2 used in the breakthrough experiments is indicated by the vertical dashed line.

The different rate of increase of unit cell size with p_{CO2} (at least up to 0.2 bar CO_2) for $Cs_{2.5}$Li-Rho compared to Li-Rho and the higher enthalpy of adsorption on $Cs_{2.5}$Li-Rho compared to Li-Rho derives from the location and the coordination behaviour of the extra-framework cations. In dehydrated Li-Rho the initial structure is strongly distorted and the Li^+ is closely coordinated to framework O atoms in 6R and 8R sites. We speculate that for the CO_2 to coordinate to Li^+ in Li-Rho the cations must move away from these oxygen atoms, with an associated energy cost, and then the flexible structure may adopt a larger unit cell. In dehydrated $Cs_{2.5}$Li-Rho, the presence of the large Cs^+ cation in the D8R site results in a larger unit cell and a less distorted framework structure than in dehydrated Li-Rho. As a result, the Li^+ cations in 6R sites may coordinate the CO_2 without the need for strong change in the framework, giving higher initial isosteric heats and a relatively flat heat/uptake profile.

The breakthrough curves on the Li-Rho and $Cs_{1.8}$Li-Rho can be compared in light of these observations. At the partial pressure of CO_2 in the gas stream, 0.05 bar, the window size of Li-Rho is smaller than that of the $Cs_{2.5}$Li-Rho and will also be smaller than that of the $Cs_{1.8}$Li-Rho measured in the breakthrough curve. CO_2 can pass through the window for Li and $Cs_{1.8}$Li-Rho, albeit with some restrictions in Li-Rho, whereas methane uptake is highly restricted for the $Cs_{1.8}$Li-Rho and not possible for the Li-Rho. At equilibrium in the breakthrough curves (p_{CO2} = 0.05 bar) the measured CO_2 uptake is similar on $Cs_{1.8}$Li-Rho to that on Li-Rho or $Na_{2.1}$Li-Rho, with a value of 1.45 mmol g^{-1}. The equilibrium selectivity, as measured from the analysis of the desorption curves, is very high (>200).

The trend of the kinetics of CO_2 desorption reflects the trend of the "sharpness" of the adsorption curves (Figures 6 and 8) . Li-Rho and $Na_{2.1}$Li-Rho have similar adsorption time constants of 20-30 min, while $Cs_{1.8}$Li-Rho has a significantly faster time constant of 8 min. This is because the pore window of the flexible zeolite Rho can be controlled by cation composition. We therefore envisage a route to cation controlled molecular sieving over the flexible zeolite Rho, where its adsorption shape selectivity is modified by modification of its cation composition. It should be noted that all these Rho samples adsorb CO_2 more slowly than NaA, which has a circular 8-ring window.[48]

By contrast with zeolite Rho, the large pore zeolite 13X does take up appreciable quantities of methane under similar conditions (at 298 K, 13X adsorbs 0.35 mmol g^{-1} at 0.5 bar and 0.6 mmol g^{-1} at 1 bar[49]). However, because of its high affinity for CO_2 it also shows very high CO_2/CH_4 equilibrium selectivity under the conditions examined here (see breakthrough and desorption curves, Figures S6.1 and S6.2). However, under conditions where adsorption is kinetically-controlled (for example where cycle times are very short) there could be some advantage in using zeolite Li-Rho, suitably cation-exchanged with a second cation that occupies D8R sites and results in the open windows having larger free diameters.

Furthermore, at higher CH_4 pressures, the M,Li-Rho materials may show distinct advantages. For example, at 10 bar CH_4 at 298 K the uptake on 13X approaches 3 mmol g^{-1}, whereas M,Li-Rho zeolites might still be expected to exclude CH_4 and be highly selective to CO_2, even where the latter was present at pressures well below 1 bar. Finally, the kinetics and thermodynamics of this separation will depend on the details of the crystal chemistry of the Rho adsorbent (crystal morphology, cation content, framework composition) and this gives considerable scope for tuning the adsorbent for separations under particular sets of conditions.

4. Conclusions

Li-rich Rho materials (Si/Al = 3.9) are promising for the separation of CO_2 from CH_4 in dry gas streams in terms of their capacity, selectivity and kinetics. There are enough empty windows to allow rapid motion of CO_2 molecules throughout the structure because the Li cations preferentially occupy 6R sites in the *lta* cages, away from the 8R windows.

The size of the windows can be adjusted by cation exchange of larger univalent cations into the Li-Rho. For example, inclusion of the larger Cs^+ cation results in an increase of the unit cell size and the minimum free diameter of the 8R windows. This enables modification of diffusion rates and molecular sieving effects over M,Li-Rho, although this is complicated for CO_2-containing gases because the uptake of CO_2 is accompanied by an expansion of the Rho framework and change in pore size. All M,Li-Rho materials are expected to be selective for CO_2, but when comparing Li-Rho with Cs_xLi-Rho ($x \approx 2$), at low pressures of CO_2 the small windows of Li-Rho are likely to result in higher selectivity for CO_2 over CH_4, whereas at a pressure of CO_2 of ca. 0.5 bar the window sizes will be similar, due to greater expansion of the pore size of Li-Rho.

For the CO_2/CH_4 mixture examined, the samples of Li-Rho, Na,Li-Rho and Cs,Li-Rho studied are all highly selective. The faster adsorption on a sample of $Cs_{1.8}$Li-Rho results in a longer time for CO_2 breakthrough as a result of its slightly larger pore size. This demonstrates that modification of the pore size *via* changes in the cation composition can tune the adsorbent properties. It is likely that the properties of other flexible zeolites can be modified in a similar way.

Supporting Information

The supporting Information is available free of charge on the ACS Publications website at [DOI]

Details of the syntheses, ion exchange conditions, adsorption isotherms and structural and refinement details, including crystallographic cif files.

The research data supporting this publication can be accessed at http://dx.doi.org/10.17630/ea4fd63c-ca29-42b1-8f24-77e911ffb832

Corresponding Author

*E-mail: paw2@st-andrews.c.uk; Tel.: +44 1334 463793

Acknowledgements

The authors thank the EPSRC for funding (AMPGas EP/J02077X/1, A.G.G., S.B., P.A.W.; and a PhD+ scholarship for M.M.L.)]. We also thank Professor Chiu C. Tang for assistance at

the I-11 beamline at the Diamond Light Source (DLS) and DLS for beamtime (Award Nos. EE9027-1 and EE11830-1), and Johnson Matthey Plc. for use of porosimetry equipment.

References

[1] Epiepang, F. E.; Li, J. B.; Liu, Y. S.; Yang, R. T. Low Pressure Performance Evaluation of CO_2, H_2O and CH4 on Li-LSX as a Superior Adsorbent for Air Pre-Purification. *Chem. Eng. Sci.* **2016**, *147*, 100-108.

[2] Tagliabue, M.; Farruseng, D.; Valencia, S.; Aguado, S.; Ravon, U.; Rizzo, C.; Corma, A.; Mirodatos, C. Natural Gas Treating by Selective Adsorption: Material Science and Chemical Engineering Interplay. *Chem. Eng. J.* **2009**, *155*, 553-566.

[3] Cavenati, S.; Grande, C. A.; Rodrigues, A. E. Separation of $CH_4/CO_2/N_2$ Mixtures by Layered Pressure Swing Adsorption for Upgrade of Natural Gas. *Chem. Eng. Sci.* **2006**, *61*, 3893-3906.

[4] Bacsik, Z.; Cheung, O.; Vasiliev, P.; Hedin, N. Selective Separation of CO_2 and CH_4 for Biogas Upgrading. *Applied Energy* **2016**, *162*, 613-621.

[5] Cavenati, S.; Grande, C. A.; Rodrigues, A. E. Upgrade of Methane from Landfill Gases by Pressure Swing Adsorption. *Energy and Fuels* **2005**, *19*, 2545-2555.

[6] Choi, S.; Drese, J. H.; Jones, C. W. Adsorbent Materials for Carbon Dioxide Capture from Large Anthropogenic Point Sources. *Chemsuschem* **2009**, *2*, 796-854.

[7] Moliner, M.; Martinez, C.; Corma, A. Synthesis Strategies for Preparing Useful Small Pore Zeolites and Zeotypes for Gas Separations and Catalysis. *Chem. Mater*. **2014**, *26*, 246-258.

[8] Cheung, O.; Hedin, N. Zeolites and Related Sorbents with Narrow Pores for CO_2 Separation from Flue Gas. *RSC Adv.* **2014**, *4*, 14480-14494.

[9] Palomino, M.; Corma, A.; Rey, F.; Valencia, S. New Insights on CO_2-Methane Separation using LTA Zeolites with Different Si/Al Ratios and a First Comparison with MOFs. *Langmuir* **2010**, *26*, 1910-1917.

[10] Bacsik, Z.; Cheung, O.; Vasiliev, P.; Hedin, N. Selective Separation of CO_2 and CH_4 for Biogas Upgrading on Zeolite NaKA and SAPO-56. *Applied Energy* **2016**, *162*, 613-621.

[11] Hudson, M. R.; Queen, W. L.; Mason, J. A.; Fickel, D. W.; Lobo, R. F.; Brown, C. M.; Unconventional, Highly Selective CO_2 Adsorption in Zeolite SSZ-13. *J. Am. Chem. Soc*. 2012, 134, 1970-1973.

[12] Fischer, M.; Bell, R. G. Identifying Promising Zeolite Frameworks for Separation Applications: A Building-Block-Based Approach. *J. Phys. Chem. C* **2013**, *117*, 17099-17110.

[13] Baerlocher, Ch.; McCusker, L. B.; Olson, D. H. Atlas of Zeolite Framework Types 6th Ed. Elsevier, **2007**.

[14] Pluth, J. J.; Smith, J. V. Accurate Re-determination of Crystal Structure of Dehydrated Zeolite A. Absence of Near Zero Coordination of Sodium – Refinement of Si,Al;-Ordered Superstructure. *J. Am. Chem. Soc.* **1980**, *102*, 4704-4708.

[15] Pluth, J. J.; Smith, J. V. Crystal Structure of Dehydrated Potassium-Exchanged Zeolite A. Absence of Supposed Zero-Coordinated Potassium. Refinement of Si,Al-Ordered Superstructure. *J. Phys. Chem.* **1979**, *83*, 741-749.

[16] Pluth, J. J.; Smith, J. V. Crystal Structure of Dehydrated Ca-Exchanged Zeolite A - Absence of Near-Zero Coordinate Ca^{2+} - Presence of Al Complex. *J. Am. Chem. Soc.* **1983**, *105*, 1192-1195.

[17] Plant, D. F.; Maurin, G.; Jobic, H.; Llewellyn, P. L. Molecular Dynamics Simulation of the Cation Motion upon Adsorption of CO_2 in Faujasite Zeolite Systems. *J. Phys. Chem. B* **2006**, *110*, 14372-14378.

[18] Liu, Q.; Mace, A.; Bacsik, Z.; Sun, J.; Laaksonen, A.; Hedin, N. NaKA Sorbents with High CO_2-over-N_2 Selectivity and High Capacity to Adsorb CO_2. *Chem. Commun.* **2010**, *46*, 4502-4504.

[19] Mace, A.; Hedin, N.; Laaksonen, A. Role of Ion Mobility in Molecular Sieving of CO_2 over N_2 with Zeolite NaKA. *J. Phys. Chem. C* **2013**, *117*, 24259-24267.

[20] Shang, J.; Li, G.; Singh, R.; Gu, Q.; Nairn, K. M.; Bastow, T. J.; Medhekar, N.; Doherty, C. M.; Hill, A. J.; Liu, J. Z. *et al.* Discriminative Separation of Gases by a "Molecular Trapdoor" Mechanism in Chabazite Zeolites. *J. Am. Chem. Soc*. **2012**, *134*, 19246-19253.

[21] Shang, J.; Li, G.; Singh, R.; Xiao, P.; Liu, J. Z.; Webley, P. A. Determination of Composition Range for "Molecular Trapdoor" Effect in Chabazite Zeolite. *J. Phys. Chem. C* **2013**, *117*, 12841-12847.

[22] Lozinska, M. M.; Mangano, E.; Mowat, J. P. S.; Shepherd, A.; Howe, R. F.; Thompson, S. P.; Parker, J. E.; Brandani, S.; Wright, P. A. Understanding Carbon Dioxide Adsorption on Univalent Cation Forms of the Flexible Zeolite Rho at

Conditions Relevant to Carbon Capture from Flue Gases. *J. Am. Chem. Soc*. **2012**, *134*, 17628-17642.

[23] Lozinska, M. M., Mowat, J. P. S.; Wright, P. A.; Thompson, S. P.; Jorda, J. L.; Palomino, M.; Valencia, S.; Rey, F. Cation Gating and Relocation during the Highly Selective "Trapdoor" Adsorption of CO_2 on Univalent Cation Forms of Zeolite Rho. *Chem. Mater*. **2014**, 26, 2052-2061.

[24] Palomino, M.; Corma, A.; Jorda, J.; Rey, F.; Valencia, S. Zeolite Rho: A Highly Selective Adsorbent for CO_2/CH_4 Separation Induced by a Structural Phase Modification. *Chem. Commun*. **2012**, *48*, 215-217.

[25] Greenaway, A. G.; Shin, J.; Cox, P. A.; Shiko, E.; Thompson, S. P.; Brandani, S.; Hong, S. B.; Wright, P. A. Structural Changes of Synthetic Paulingite (Na,H-ECR-18) upon Dehydration and CO_2 Adsorption. *Zeit. Krist. – Cryst. Mat.* **2015**, *230*, 223-231.

[26] Guo, P.; Shin, J.; Greenaway, A. G.; Gi Min, J.; Su, J.; Choi, H. J.; Liu, L.; Cox, P. A.; Hong, S. B.; Wright, P. A. *et al.* A Zeolite Family with Expanding Structural Complexity and Embedded Isoreticular Structures. *Nature* **2015**, *524*, 74-78.

[27] Robson, H. E.; Shoemaker, D. P.; Ogilvie, R. A.; Manor, P. C. Synthesis and Crystal Structure of Zeolite Rho—a New Zeolite Related to Linde Type A. In '*Molecular Sieves*' Meier, W. M., Uytterhoeven, J. B. Eds.; American Chemical Society: Washington D.C. **1973**; *Adv. Chem. Ser. No.* 121, 106.

[28] Kapoor, A.; Yang, R. T. Kinetic Separation of Methane – Carbon Dioxide Mixture by Adsorption on Molecular Sieve Carbon. *Chem. Eng. Sci.* **1989**, *44*, 1723 – 1733.

[29] Johnson, G. M.; Reisner, B. A.; Tripathi, A.; Corbin, D. R.; Toby, B. H.; Parise, J. B. Flexibility and Cation Distribution upon Lithium Exchange of Aluminosilicate and

Aluminogermanate Materials with the RHO Topology. *Chem. Mater.* **1999**, *11*, 2708-2787.

[30] Frisch, H.L.; Hammersley, J. M.; Welsh, D. J. A. Monte Carlo Estimates of Percolation Probabilities for Various Lattices. *Phys. Rev.* **1962**, *126*, 949-951.

[31] Keffer, D.; McCormick, A. V.; Davis, H. T. Diffusion and Percolation on Zeolite Sorption Lattices. *J. Phys. Chem*. **1996**, *100*, 967-973.

[32] Vrabe, J.; Stoll, J.; Hasse, H. A Set of Molecular Models for Symmetric Quadrupolar Fluids. *J. Phys. Chem. B* **2001**, *105*, 12126 – 12133.

[33] Chatelain T.; Patarin J.; Fousson E.; Soulard M.; Guth J. L.; Schulz P. Synthesis and Characterization of High-Silica Zeolite RHO Prepared in the Presence of 18-Crown-6 Ether as Organic Template. *Microporous Mater.* **1995**, *4*, 231-238.

[34] Robson, H.E.; Shoemaker, D. P.; Ogilvie, R.A.; Manor, P. C. Synthesis and crystal structure of zeolite Rho - a new zeolite related to Linde type A. *Adv. Chem. Ser.*, **1973**, *121*, 106-115.

[35] Pera-Titus, M.; Palomino, M.; Valencia, S.; Rey, F. Thermodynamic Analysis of Framework Deformation in Na,Cs-RHO Zeolite upon CO_2 Adsorption. *Phys. Chem. Chem. Phys.* **2014**, *16*, 24391-24400.

[36] Thompson, S. P.; Parker, J. E.; Potter, J.; Hill, T. P.; Birt, A.; Cobb, T. M.; Yuan, F.; Tang, C. C. Beamline I11 at Diamond: A New Instrument for High Resolution Powder Diffraction. *Rev. Sci. Instrum.* **2009**, *80*, 075107-9.

[37] Thompson, S. P.; Parker, J. E.; Marchal, J.; Potter, J.; Birt, A.; Yuan, F.; Fearn, R. D.; Lennie, A. R.; Street, S. R.; Tang, C. C. Fast X-ray Powder Diffraction on I11 at Diamond. *J. Synchr. Radiation* **2011**, *18*, 637-648.

[38] Larson, A. C.; Von Dreele, R. B. *General Structure Analysis System (GSAS)*; Los Alamos National Laboratory, USA, 1994.

[39] Hu X.; Brandani S.; Benin A. I., Willis R. R. Development of a Semi-Automated Zero Length Column Technique for Carbon Capture Applications: Study of Diffusion Behaviour of CO_2 in MOFs. *Ind. Eng. Chem. Res.* **2015**, *54*, 5777-5783.

[40] Hu, X.; Mangano, E.; Friedrich, D.; Ahn, H.; Brandani, S. Diffusion Mechanism of CO_2 in 13X Zeolite Beads. *Adsorption* **2014**, *20*, 121-135.

[41] Friedrich, D.; Brandani, S.; Ahn, H. Efficient Simulation and Acceleration of Convergence for a Dual Piston Pressure Swing Adsorption System. *Ind. Eng. Chem. Res.* **2013**, *52*, 8897-8905.

[42] Dang, W.; Friedrich, D.; Brandani, S. Characterisation of an Automated Dual Piston Pressure Swing Adsorption (DP-PSA) System. *Energy Procedia*, **2013**, *37*, 57-64.

[43] Banu, A.M.; Friedrich, D.; Brandani, S.; Düren, T. A Multiscale Study of MOFs as Adsorbents in H_2 PSA Purification. *Ind. Eng. Chem. Res.* **2013**, *52*, 9946-9957.

[44] Luberti, M.; Friedrich, D.; Brandani, S.; Ahn, H. Design of a H_2 PSA for Co-generation of Ultrapure Hydrogen and Power at an Advanced Integrated Gasification Combined Cycle with Pre-Combustion Capture. *Adsorption* **2014**, *20*, 511-524.

[45] Friedrich, D.; Mangano, E.; Brandani, S. Automatic Estimation of Kinetic and Isotherm Parameters from ZLC Experiments. *Chem. Eng. Sci.* **2015**, *126*, 616-624.

[46] Parise, J. B.; Abrams, L.; Gier, T. E.; Corbin, D. R.; Jorgensen, J. D.; Prince, E. Flexibility of the Framework of Zeolite Rho: Structural Variation from 11 to 573 K. A Study using Neutron Powder Diffraction Data. *J. Phys. Chem.* **1984**, *88*, 2303-2307.

[47] Llewellyn, P. L.; Maurin, G. Gas Adsorption Microcalorimetry and Modelling to Characterise Zeolites and Related Materials. *CR Acad Sci. II C* **2005**, *8*, 283-302.

[48] (a) Kärger, J.; Pfeifer, H.; Stallmach, F.; Feoktistova, N.N.; Zhdanov, S. P. ^{129}Xe and ^{13}C P.F.G. N.M.R. Study of the Intra-Crystalline Self-Diffusion of Xe, CO_2 and CO. *Zeolites* **1993**, *13*, 50-55.; (b) Ruthven, D. M. Diffusion of Xe and CO_2 in 5A Zeolite Crystals. *Zeolites* **1993**, *13*, 594.

[49] Cavenati, S.; Grande, C. A.; Rodrigues, A. E. Adsorption Equilibrium of Methane, Carbon Dioxide, and Nitrogen on Zeolite 13X at High Pressures. *J. Chem. Eng. Data* **2004**, *49*, 1095-1101.